Theor Chem Account (2008) 119:477–487
DOI 10.1007/s00214-007-0408-1

REGULAR ARTICLE

Car-Parrinello molecular dynamics simulations and EPR property calculations on aqueous ubisemiquinone radical anion

James R. Asher · Martin Kaupp

Received: 16 November 2007 / Accepted: 28 December 2007 / Published online: 19 January 2008

Abstract Car-Parrinello molecular dynamics (CPMD) simulations have been performed on ubisemiquinone radical anion in aqueous solution. The different types of hydrogen bonding formed between the semiquinone and the solvent were studied in terms of frequency and directionality, in comparison with the parent benzosemiquinone radical anion. The EPR parameters (g-tensors and hyperfine coupling constants) were obtained from quantum chemical property calculations performed on snapshots along the MD trajectory, and the contributions of different solvation effects to the EPR parameters have been evaluated. The influence of the anion's conformational behaviour was examined, including the orientation-dependent effects of hyperconjugation on side-chain hyperfine coupling.

Keywords Car-Parrinello molecular dynamics · EPR parameters · g-tensors · Hydrogen bonding dynamics · Hyperfine coupling constants · Ubisemiquinone

1 Introduction

Quinones and their reduced forms (semiquinones and quinols) occur in all life-forms as antioxidants and electron transfer agents [1–3]. The most important compound of this class is ubiquinone (UQ), so named for its ubiquity. It is a vital cofactor in, e.g., photosynthesis and respiration. Electron paramagnetic resonance (EPR) spectroscopy has proven itself an important tool for studying ubisemiquinone and other anionic semiquinone radicals, and numerous EPR studies have been performed on semiquinones [4,5]. The EPR parameters (g-tensors and hyperfine coupling constants) are very sensitive to intermolecular interactions such as hydrogen bonding, and thus give valuable data about the molecular environment of the bioradical. This is particularly useful for investigating the hydrogen bonding interactions at an enzyme reaction centre, which serve not only to keep the (semi)quinone cofactor in place, but also to modify the quinone/semiquinone redox potential.

To interpret this data, it is desirable to have a thorough understanding of the effects of hydrogen bonding on the EPR parameters. Computational chemistry can play a useful role here, as techniques based on density functional theory (DFT) may be used to calculate the EPR parameters even for large, chemically relevant radical systems [6]. The computation of hyperfine tensors for π-radicals has become more or less routine, using DFT with hybrid functionals [7]. Semiquinones have been prominent targets in such applications [8–19]. More recently, DFT calculations of electronic g-tensors have reached an accuracy that make them particularly suitable for applications to bioradicals [20]. Indeed, semiquinone radical anions have been among the first serious applications of DFT methods to g-tensor calculations, giving insight into a large variety of factors that influence the spectroscopic parameters, in particular with respect to the solvent or protein environment [21–28].

All these initial calculations have been done using static structures, typically generated by computational optimization, but sometimes (especially when investigating enzyme binding sites) constrained to match experimental structural data from, e.g., X-ray diffraction. Necessarily, this approach omits dynamical effects, such as vibration and the fluctuating number, orientations and lengths of hydrogen bonds. This omission can be rectified by performing molecular dynamics (MD) simulations, in which the evolution of a system over time is simulated. We have previously used Car-Parrinello

J. R. Asher · M. Kaupp (✉)
Institut für Anorganische Chemie, Universität Würzburg,
Am Hubland, 97074 Würzburg, Germany
e-mail: kaupp@mail.uni-wuerzburg.de

molecular dynamics [29] (CPMD) simulations to examine the interaction of aqueous benzosemiquinone radical anion ($BQ^{\bullet-}$) with the solvent water molecules and the effect of solvation and dynamics on EPR parameters [30–32] (cf. refs. [33–41] for examples of further studies that include dynamical effects in DFT calculations of EPR parameters). In this paper we extend the use of this methodology to the biologically more relevant ubisemiquinone radical anion. First results are reported here for solvation analysis, *g*-tensors and hyperfine couplings calculated from the MD trajectory of ubisemiquinone in aqueous solution.

2 Computational details

We performed Car-Parrinello MD simulations using the CPMD code (version 3.7.1) [42] on a system comprising ubisemiquinone radical anion in a periodic box (of size $14.0 \times 13.0 \times 16.5$ Å) with 92 water molecules. As the full molecule would be too large to perform a long enough simulation on, we replaced the isoprenyl side-chain with an ethyl group (cf. Fig. 1). No counterions were added or special measures were taken to negate the effect of image charges, as the dielectric effects of the highly polar solvent are expected to effectively screen the electrostatic interactions between neighbouring cells. The BLYP functional [43,44] was used to calculate the electronic energy. BLYP is well validated for simulations in aqueous media and known to provide a reasonable hydrogen-bonding framework [45], in spite of some shortcomings when it comes to details [46]. Our previous study of aqueous $BQ^{\bullet-}$ study was also performed using BLYP, and thus comparison between the two semiquinones is best done at this level.

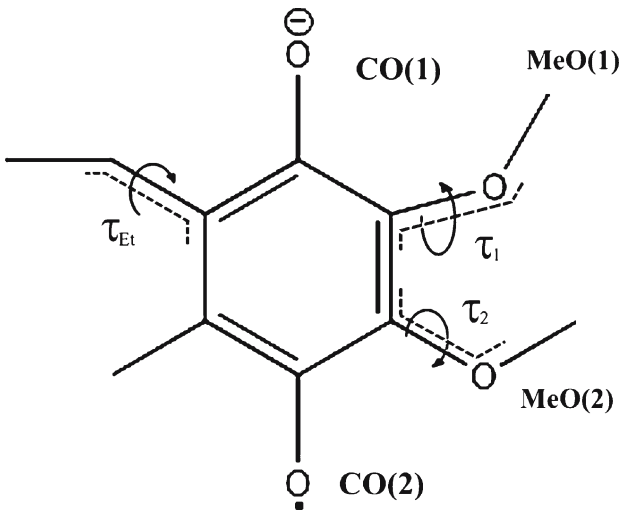

Fig. 1 Definition of groups and torsional angles in ubisemiquinone. *Dashed lines* indicate the three bonds defining a torsional angle

A planewave basis with 70 Ry cutoff energy was used with Troullier-Martins type norm-conserving pseudopotentials [47]. We used a timestep of 7 a.u. (0.17 fs), although for a short period of the preproduction trajectory the timestep was switched to 5 a.u. to examine the effect on energy conservation; 7.99 ps of simulation was produced, of which we discarded 5.38 ps as an equilibration period and took the latter 2.61 ps as a production run.

This is so far a significantly shorter production run than that simulated for the smaller (and thus computationally cheaper) benzosemiquinone radical anion, and thus the data obtained from its analysis will be less statistically reliable. Longer simulations are desirable, due to lower symmetry and the need to sample the different conformations possible. Work along these lines is currently in progress.

In this paper we use the following notation for the atoms and groups of $UQ^{\bullet-}$. As per convention, C_{ipso} refers to the carbonyl carbons and C_{ortho} to the other ring carbon atoms. The oxygen atoms are labelled with their functional group as subscripts: O_{CO} and O_{MeO} thus refer to the carbonyl and methoxy oxygen atoms, respectively. Unlike benzosemiquinone, however, the two CO groups are not equivalent, and neither are the MeO groups. The CO group adjacent to the isoprenoid tail (ethyl group in the model) is denoted as CO(1), and the MeO group next to it (and opposite the isoprenoid group) is denoted as MeO(2). The CO and MeO groups adjacent and opposite to the Me group are denoted as MeO(2) and CO(2), respectively. The torsional angles of the side groups may be defined either as $D(X_b–X_a–C_{ortho}–C_{ipso})$ or $D(X_b–X_a–C_{ortho}–C_{ortho})$. We choose the latter, and use the labels τ_1, τ_2 and τ_{Et} for the two MeO groups and the ethyl group respectively. This is illustrated in Fig. 1.

The criteria for hydrogen bond recognition are as follows. Hydrogen bonding to carbonyl oxygen requires $r[H \cdots O] < 2.25$ Å and $\angle(O–H \cdots O) > 90°$. For methoxy oxygen, we define the "loose" critera the same way, and for the "strict" criteria additionally exclude water molecules already H-bonded to carbonyl oxygen. For "T-stacked" H-bonding to the C_6 ring, the "loose" criteria require that $\angle(O–H \cdots C) > 120°$ and $\angle(H \cdots C \cdots [m]) > 135°$, where [m] is the midpoint of the C_6 ring, and that the hydrogen be closer to carbon than to a carbonyl oxygen. The "tight" criteria additionally exclude water molecules H-bonded to methoxy oxygens.

Radial distribution functions (RDFs) are plotted for protons H-bonded to oxygen centres of $UQ^{\bullet-}$. This was done by dividing the radial frequency of such protons by a radial area element (taken to be $4\pi r^2$) and normalizing to the bulk density of water molecules. (The RDF measures variation in solvent density according to distance from the molecule, and ideally converges to 1 at large distances.)

Calculation of EPR parameters was performed by taking snapshots from the trajectory at regular intervals of 13.5 fs and calculating the electronic structure for molecular clusters

at DFT level with the TURBOMOLE program [48,49] (construction of the clusters will be discussed in the next section). The electronic structure calculations for these clusters were performed at the BP86/DZVP [43,50,51] level for g-tensors and B3LYP/EPR-II [52–54] for hyperfine coupling constants. The Kohn–Sham orbitals were then passed to the MAG/ReSpect magnetic resonance calculation package [55]. The g-tensors were calculated using a second-order perturbation–theoretical approach [56,57], the atomic meanfield approximation for spin–orbit integrals [58], and a common gauge origin located midway between the carbonyl oxygens. (Semiquinone g-tensors do not, however, tend to be very sensitive to gauge position.)

3 Results and discussion

Frequency of hydrogen bonding

Table 1 shows the frequency of particular types of hydrogen bonds, under "strict" criteria, and also the relative frequency of a particular number of each type of hydrogen bonding present. (By "frequency" we mean the fraction of snapshots in which that number of H-bonds is found.) As with benzosemiquinone radical anion, the most extensively occurring type of hydrogen bonding is to the carbonyl oxygens, with four or five such H-bonds being most common, and the simulation average being 4.6 (the number computed for benzosemiquinone at the same level is 4.7 [30]), or 2.3 to each oxygen. However, the radial distribution function (see Fig. 2) for the first solvation sphere around O_{CO} is broader and has a smaller maximum value than found in our simulations [30] of $BQ^{\bullet-}$. Furthermore, the H-bonds are somewhat longer: $g(r)$ is at a maximum at around 1.95 Å (1.75 Å for $BQ^{\bullet-}$). It appears that the presence of substituents on the C_6 ring does not substantially decrease the number of hydrogen bonds to the carbonyl oxygen atoms, but does (by steric repulsion) cause

Table 1 H-bond numbers

Number of H-bonds	Occurrence for H-bonds of type (%)		
	$H\cdots O_{OC}$	$H\cdots O_{MeO}$	$H\cdots C_6$
0	–	31	64
1	–	47	25
2	4	20	10
3	14	3	1
4	25	–	–
5	38	–	–
6	15	–	–
7	5	–	–
Average number	4.6	0.9	0.5

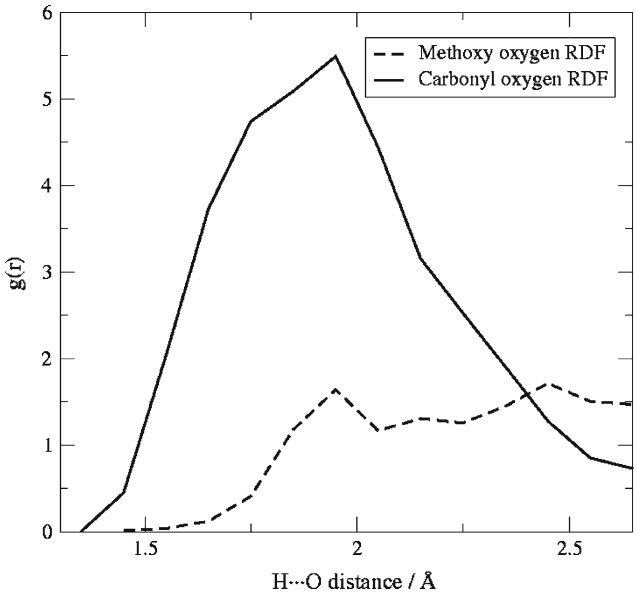

Fig. 2 Radial distribution functions (RDFs) of water molecules H-bonded to carbonyl oxygen and methoxy oxygen atoms ("loose" criteria)

significant elongation of these hydrogen bonds. This effect has been noted in static calculations on ubisemiquinone, and arises when multiple H-bonds are present to the same oxygen [26]. At low numbers of hydrogen bonds, the H-bond distance is significantly shorter, as the solvent molecules have enough room to avoid steric interaction with the side groups. (Even in the absence of bulky side groups, H-bonds to semiquinones are shorter the fewer solvent molecules there are [59]. However, the effect is more drastic in the case of $UQ^{\bullet-}$, due to the steric factors.)

The location of the RDF peak is subject to a degree of statistical noise, and varies somewhat according to the resolution with which the RDF is plotted, but fitting a gaussian function to the 1.65–2.05 Å region gave a peak RDF value of 5.4 at ∼1.89 Å. This is in line with frozen ^{i}PrOH ENDOR data suggesting H-bond lengths of 1.89 and 1.94 Å to the two carbonyl oxygen atoms [60] (H-bond lengths are very similar in water—1.76 Å [61]—and ^{i}PrOH—1.78 Å [60] in the case of $BQ^{\bullet-}$, so in the absence of aqueous data for $UQ^{\bullet-}$, it is probably safe to compare to ^{i}PrOH data instead). The computed values are longer than the H-bond distances found in many of the earlier theoretical studies (1.79 Å for $UQ^{\bullet-}$ + 4MeOH at B3LYP/EPR-II [62], 1.78–1.89 Å for $UQ^{\bullet-}$ + $4H_2O$ at BLYP/DZVP [21]). However, recent static $UQ^{\bullet-}$ + $4H_2O$ calculations at the BP86/DZVP level found both a short (1.75–1.77 Å) and a long (2.10–2.12 Å) hydrogen bond to each carbonyl oxygen [26], giving an average H-bond length very similar to our RDF peak. It would appear that the effects of steric repulsion on H-bond length are significantly underestimated if too few solvent molecules are included in the first solvation sphere. This also explains why an MM-MD

simulation of $UQ^{\bullet-}$, which only found 2.4 water molecules in the first solvation sphere (an unrealistically low value), found an RDF peak at 1.77 Å [63].

If the simulation were long enough, the differences in hydrogen bonding to the two asymmetric carbonyl groups could be estimated. However, our production run is not long enough for this. (Even in our longer 6.4 ps simulation of the benzosemiquinone radical anion [30,31], a 0.2 H-bond difference arose between the formally equivalent carbonyl groups.)

Hydrogen bonding to methoxy oxygen atoms is significant, although a far weaker interaction than H-bonding to carbonyl oxygen. This is because, in resonance structure terms, the negative charge is located on O_{CO} to a significant degree, but not on O_{MeO}: the interaction of O_{MeO} with the π-system involves donation of the oxygen lone-pair to form a double-bond with the C_6 ring, resulting in a mesomer with formal *positive* charge on the oxygen (we may also understand this in terms of negative hyperconjugation, with an occupied oxygen lone-pair orbital delocalizing partially into the π-system). Figure 2 shows the RDF of water molecules around methoxy oxygens ("loose" criteria). A peak is seen a little under 2 Å, representing water molecules actually H-bonded to methoxy oxygen atoms. The peak further out, ~2.5 Å, represents the first solvation shell of the carbonyl oxygen atoms.

Under "loose" criteria, an average of 1.1 hydrogen bonds is found to the methoxy oxygens. Under "strict" criteria, the average number is 0.9. The most common situation is one such H-bond, followed by none, and the number at any point in the simulation ranges from 0 to 3 (and from 0 to 2 per methoxy group). Under "loose" criteria, the longest lived H-bond noted lasted for 335 fs (the longest lifetime under "strict" criteria is 214 fs). The "loose" criteria are useful for including the entire solvation sphere of the methoxy groups. However, they include some water molecules also H-bonded to carbonyl oxygens, so the "strict" criteria are necessary for examining the effects of to-methoxy hydrogen bonds in isolation.

We would expect that hydrogen bonding to carbonyl oxygen would discourage other types of H-bonds. Curiously, however, the correlation between numbers of $O_{CO}\cdots H$ and $O_{MeO}\cdots H$-bonds is positive, and the correlation with T-stacking H-bonds is ambiguous (Table 2). This is probably due to limited statistical accuracy because of the short trajectory.

We also find hydrogen bonds to the C_6 ring in the ubisemiquinone simulation, as we did for benzosemiquinone [30,31]. However, the incidence of these is lower: an average of 0.7 per snapshot for loose criteria, 0.5 for strict (for $BQ^{\bullet-}$, 1.1 are found on average), and the most common situation is for no T-stacked H-bonds to form at all. We attribute this to steric obstruction from the side groups, preventing T-stacked H-bonds from forming.

Table 2 Correlation of hydrogen bonds to carbonyl oxygen with other H-bond types (strict criteria)

$n(H\cdots O_{CO})$	$n(H\cdots O_{MeO})$	$n(H\cdots C_6)$
2	(0.2)	(0.4)
3	0.3	0.4
4	0.5	0.5
5	0.5	0.6
6	0.6	0.3
7	(0.1)	(0.0)

Values in parentheses indicate statistically less reliable data

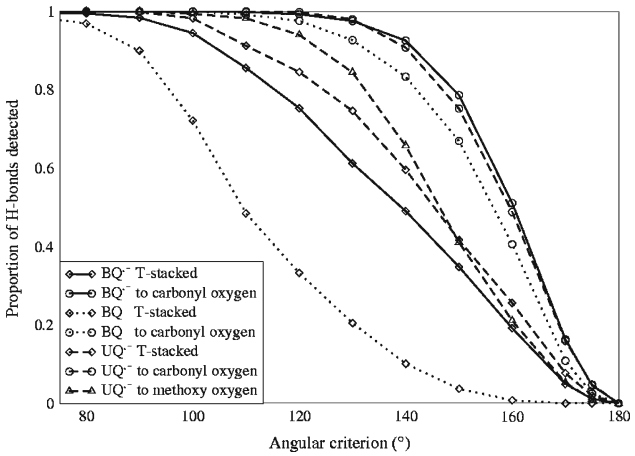

Fig. 3 Directionality graph (inverse cumulative frequency graph for angle definition) for various hydrogen bond types

Hydrogen bond directionality

In order to assess the strength of the different hydrogen bond types, we have computed and plotted (Fig. 3) a quantity we refer to as "directionality", for all H-bond types to BQ, $BQ^{\bullet-}$ and $UQ^{\bullet-}$. This is the number of hydrogen bonds detected by setting the angular criterion to $\angle(O\text{–}H\cdots X) > \theta$, normalized to the number detected when $\theta = 0°$ (i.e. without the angular criterion applying). As θ is increased, the number of hydrogen bonds detected will decrease, and will eventually fall to 0 when $\theta = 180°$. Plotting the directionality against θ thus gives an (inverted) cumulative frequency graph of $\angle(O\text{–}H\cdots X)$ for nearby water molecules. The stronger a H-bonding interaction is, the more the nearby O–H bonds will orient themselves towards the H-bond acceptor, increasing $\angle(O\text{–}H\cdots X)$. We can assess this by looking at the median angle for each H-bond type, i.e. the value of θ for which the directionality is 0.5.[1]

[1] Taking directionality as a measure of H-bond strength is of course a simplification: the presence of other nearby electrostatic charges, as well as the steric accessibility of the H-bond acceptor, are likely to have an effect.

Hydrogen bonds to semiquinone carbonyl oxygen atoms are very directional—almost all nearby water molecules are included up to $\theta = 120°$. The median angle for both $UQ^{\bullet-}$ and $BQ^{\bullet-}$ is around 160°, an almost linear H-bond. H-bonds to O_{CO} for neutral BQ are less directional, with a median angle of 157°. H-bonds to O_{MeO} of ubisemiquinone are considerably less directional—the median angle is 147°. This is partly due to hyperconjugation of charge towards the π-system, but probably also due to the close proximity of the highly negative carbonyl oxygens, which will orient nearby O–H bonds towards them.

Whereas hydrogen bonding to the carbonyl oxygen atoms looks very similar for both semiquinones, T-stacking hydrogen bonding is *more* directional to $UQ^{\bullet-}$ (median angle 146°) than to $BQ^{\bullet-}$ (139°). This we attribute to hyperconjugation with methoxy oxygens making the π-system a better H-bond acceptor in the case of $UQ^{\bullet-}$. The T-stacking interaction is very weak in the case of neutral BQ, as noted previously [19].

Structure of the semiquinone radical anion

The orientation of the ethyl group is reasonably consistent: it stays perpendicular to the plane for most of the trajectory ($\tau_{Et} = 92°$, standard deviation 21°). The methoxy group orientations are more complex, however. We have defined the dihedral angles τ_1 and τ_2 earlier; for clarity we will generally omit the sign and talk of the MeO groups pointing "up" or "down" in the z-direction. This is defined such that MeO(1) (which points consistently in one direction throughout our simulation) is pointing "up", and the ethyl group is pointing "down". We can also speak of the methoxy groups tilting "inward" towards each other ($\tau < 90°$) or "outward" away from each other ($\tau > 90°$) (if one points "out" and one "in", this means both are pointing in the same direction).

Several previous computational studies have found both methoxy groups pointing "outwards". Nonella [64] found such conformations to be most stable, with a 0.9 kJmol^{-1} difference between up/up and up/down conformers (a conformer with one inward-pointing group was 10 kJmol^{-1} higher in energy). A combined experimental and theoretical study suggested $\tau = 135°$ for both groups on the basis of semi-empirical modelling of EPR data [65]. A DFT study found the methoxy groups to be strongly out of plane, one pointing "up" and the other "down". Both groups pointed "outwards" in the gas phase, but slightly "inwards" once solvent molecules were attached [21]. A recent study examined both an "in/out" and an "out/out" conformation—both MeO groups pointing "up" in each case—and found them extremely similar in H-bond lengths and g-tensors [26]. ENDOR data in frozen ^{i}PrOH finds both groups of methoxy protons to have the same signal [60], suggesting that (a) rotation of the CH_3 groups is unhindered and quite fast even at low temperature, and (b) the conformation of the MeO groups is either symmetrical or rapidly interconverting.

During our simulation, the two MeO groups adopt an "out/in" conformation for almost the whole trajectory, which we depict in Fig. 4. Initially, for about a picosecond, MeO(1) is almost perpendicular to the ring, pointing slightly outwards (a), while MeO(2) points inwards, swinging between 0 and 60° in both the "up" and "down" directions, but generally

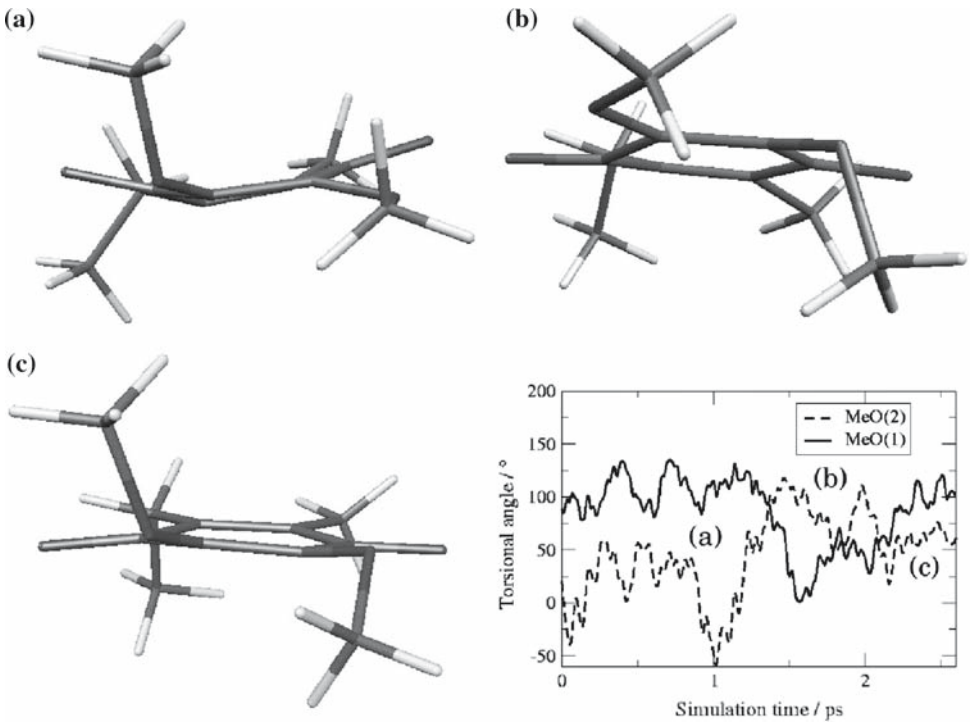

Fig. 4 Observed methoxy group conformations. *Inset graph* shows time-variation of dihedral angles (in case of MeO(2), positive dihedral indicates "down" orientation, negative indicates "up")

"down". For a brief period the conformation reverses (b), with MeO(1) swinging "inwards" (and at one point being in-plane) and MeO(2) near-perpendicular and slightly "outwards". Then the conformation returns to the initial state (c), although with MeO(2) not being particularly in-plane.

The length of our simulation is not sufficient to make any comments about which conformation is preferred in solution, or whether conformations with both MeO groups pointing "outwards" are likely to occur. Nevertheless, *at no point* do we see both MeO groups with dihedral angles of 135°, or even 120°. Only for a few femtoseconds do both τ_1 and τ_2 exceed 90°, and this is while the methoxy groups are switching between conformers. On a longer simulation it may be that a conformation with both MeO groups pointed "outwards" would be seen for significant lengths of time. But our simulation indicates that it would not be the only stable conformer.

A correlation exists between the torsional angles of the MeO groups and the number of hydrogen bonds to them. This is seen most clearly in the difference between the two groups: for about 75% of the trajectory, $\tau_1 > \tau_2$, and during this period there are an average of 0.2 H-bonds more to OMe(2) than to OMe(1). For the 25% of the trajectory where $\tau_1 < \tau_2$, OMe(1) has an average of 0.3 H-bonds more to it than OMe(2). This is what would be expected: the lower the torsional angle, the more "inwards" the OMe group points, and the more sterically accessible the oxygen lone pairs become for hydrogen bonding (we note that the effect of hydrogen bonding on orientation may be the opposite: prior static calculations found that including H-bonding to MeO groups increased the dihedral angles [21]).

The carbonyl C–O bond length averages 1.30 Å, the same value as for our $BQ^{\bullet-}$ simulations. The O–CH_3 single bonds in the methoxy groups are each 1.48 Å on average. The O–C_{ortho} bond lengths are partway between these two values, at 1.40 and 1.39 Å, reflecting a small amount of double-bond character arising from the delocalization of oxygen lone-pairs into the π-system.

This delocalization of oxygen lone-pairs onto the carbon ring will shift the oxygen closer to sp^2 hybridization, and will thus be favoured by MeO group dihedral angles close to 0° (or 180°, although this does not occur in our trajectory). The result is a weak dependence of the structure around the methoxy oxygen atoms on the corresponding dihedral angle. On average, for a methoxy group that is close to being in-plane ($\tau = 0 - 45°$), we find $\angle$(C–O–C) = 121° and d(C_{ortho}–O)=1.38 Å. For methoxy groups closer to perpendicular ($\tau > 45°$), the values are $\angle$(C–O–C) = 115° and d(C_{ortho}–O) = 1.40 Å (we can also attribute the difference in $\angle$(C–O–C) to the fact that in-plane methoxy groups are, in our trajectory, always pointing "inwards", causing steric repulsion of the methyl group from the other methoxy group).

g-Tensor results

g-Tensors have been calculated for 1.99 ps of our production run, for snapshots at regular intervals of 13.5 fs. Calculations were run on a variety of cluster definitions, to analyse different contributions to the g-tensor: (1) [lone] indicates no water molecules included in the calculation. (2) [O···H] indicates all water molecules H-bonded to any oxygen atom. Water molecules H-bonded to specific types of oxygen atoms are denoted by [O_{CO}···H] and [O_{MeO}···H] (the latter using strict criteria). (3) [T-stacked] denotes water molecules engaged in T-stacking H-bonding (strict criteria). (4) [Total] includes all water molecules H-bonded to $UQ^{\bullet-}$. (5) [x Å] denotes a cluster containing all water molecules within x Ångstroms of an oxygen or ring carbon atom of the ubisemiquinone anion. (6) "+PCM" indicates that, in addition to explicit inclusion of water molecules in the calculation, long-range dielectric effects were also treated by a polarizable continuum model [66]. Test calculations indicated that, when using PCM, a 4.25 Å cluster was reasonably well converged with regard to cluster size, to within 50 ppm in the g_x component.

The results of our g-tensor calculations are shown in Table 3. Hydrogen bonding to carbonyl oxygen atoms decreases Δg_x significantly, by 1,676 ppm (cf. [lone] vs. [O_{CO}···H]). This is a smaller absolute decrease than that observed for benzosemiquinone (2,349 ppm [19]), understandable from the lower overall spin–orbit/orbital–Zeeman contribution (the relative reduction is about the same in each case, 26% for $UQ^{\bullet-}$, 29% for $BQ^{\bullet-}$), and partly from the overall larger fraction of out-of-plane hydrogen bonding for $UQ^{\bullet-}$. T-stacking hydrogen bonds increase Δg_x slightly, by 69 ppm. Again, this is a smaller effect than that seen for $BQ^{\bullet-}$, where a 195 ppm increase is seen. This can be mostly attributed to a smaller number of T-stacked hydrogen bonds being present in the case of $UQ^{\bullet-}$.

Table 3 g-Shift-tensors for various cluster definitions (in ppm)

Cluster criterion	Δg_x	Δg_y	Δg_z	Δg_{iso}
[lone]	6,473	3,399	137	3,336
[lone + PCM]	5,768	3,247	120	3,045
[T-stacking]	6,542	3,423	144	3,369
[O_{MeO}···H]	6,441	3,402	141	3,328
[O_{MeO}···H] (2)	6,477	3,403	139	3,339
[O_{CO}···H]	4,797	3,081	101	2,659
[O···H]	4,776	3,083	107	2,655
[Total]	4,824	3,109	115	2,682
[Total + PCM]	4,651	3,080	109	2,613
[4.25 Å + PCM]	4,355	3,032	143	2,506
Exp. (^{i}PrOH)[a]	3,900	2,940	220	2,353

Deviations from the free-electron value in units of 10^{-6}
[a] Ref. [60]

A factor new to ubisemiquinone is the presence of to-methoxy H-bonds. These appear to show competing effects on the g-tensor. Adding H-bonds to O_{MeO} increased g_x by about 200 ppm in static calculations [21]. In our calculations, however, $O_{MeO}\cdots H$ interactions *decrease* g_x (cf. $[O_{MeO}\cdots H]$ vs. [lone] or $[O\cdots H]$ vs. $[O_{CO}\cdots H]$). It seems that the hydrogen bonds themselves have a slight positive effect on g_x, but the water molecules involved also have a dielectric effect on the carbonyl oxygen, stabilizing negative charge there and decreasing g_x in the same manner as H-bonds to carbonyl oxygen (but much more weakly). Presumably this balance of effects exists with T-stacking H-bonds as well, but the positive effect on g_x is much stronger than the weak dielectric effect in that case. We think the "positive effect" (increase of g_x) of to-methoxy H-bonds shows up clearly in static calculations because they tend to locate the H-bonded water molecules further from the carbonyl oxygens. By inspection of our results, it appears that $O_{MeO}\cdots H$-interacting water molecules only increase g_x when quite far away from the carbonyl oxygens, when the dielectric effect is weaker. To demonstrate this, we excluded from the $[O_{MeO}\cdots H]$ cluster all water molecules within 2.7 Å of a carbonyl oxygen, and labelled this $[O_{MeO}\cdots H]$ (2). The result is a miniscule increase of Δg_x, rather than a decrease.

Comparison with experiment is complicated by the lack of EPR data on aqueous ubisemiquinone anion. Static calculations on aqueous and alcoholic g-tensors do not differ significantly [21], and g-tensors for $BQ^{\bullet-}$ in H_2O [42] and ^{i}PrOH [67] are identical to within experimental accuracy. So we will tentatively compare our [4.25 Å + PCM] data with frozen ^{i}PrOH EPR results [68]. (We use this rather than the $UQ^{\bullet-}$ ^{i}PrOH data from Ref. [67] for reasons we will detail below.) As with benzosemiquinone and static calculations using the same BP86-based methodology, we find a significant overshoot in Δg_x: 4,355 ppm, compared to an experimental value of 3,900 ppm. The Δg_y component is reasonably accurate at 3,032 ppm (exp. 2,940 ppm). As with $BQ^{\bullet-}$, Δg_z is overshot somewhat (143 vs. −220 ppm; this overestimate also occurs in static calculations [21], possibly reflecting artefacts from neglect of two-electron gauge corrections).

As with benzosemiquinone [31], the effects of dynamics seem to be to increase Δg_x somewhat. The $[O_{OC}\cdots H]$ cluster has $\Delta g_x = 4{,}797$ ppm. Approximately equivalent static calculations tend to have lower values: for $UQ^{\bullet-} + 4H_2O$ and an "out/out" conformation of the MeO groups, $\Delta g_x = 4{,}436$ ppm, increasing to 4,622 ppm on addition of two more water molecules. Other calculations found $\Delta g_x =$ 4,642 or 4,695 ppm for $UQ^{\bullet-} + 4H_2O$ [26]. This indicates that static calculations may benefit from some error compensation, with the overestimate of Δg_x from DFT errors [21,26,56] being partially cancelled by the underestimate of Δg_x from omission of dynamics. However, the difference is quite small, on the order of 100–300 ppm, whereas in the case of $BQ^{\bullet-}$, the difference was around ∼800 ppm [31]. As a result, when further solvation effects are taken into account (in the [4.25 Å + PCM] cluster), our ubisemiquinone Δg_x drops below the static calculation values, and the result is in slightly better agreement with experiment than static calculations have achieved. This contrasts with benzosemiquinone anion, for which our large-cluster dynamical results gave slightly poorer agreement with experiment than static calculations (when employing otherwise identical computational protocols). The improvement on static calculation results may be purely fortuitous, however—we have not yet sampled enough of the conformational phase space of the molecule, and the average Δg_x might increase (or decrease) if taken over a longer trajectory. It is curious that our dynamical values are significantly further from experiment for $BQ^{\bullet-}$ (ca. 800 ppm or ca. 19% [31]) than for $UQ^{\bullet-}$ (ca. 450ppm or ca. 12%). Previous studies (based on static calculations [21,26,56]) have suggested that the error in Δg_x is systematic enough to be correctable by scaling down the value by about 10%. Our current dynamical results on ubisemiquinone fit this expectation well, whereas the $BQ^{\bullet-}$ would need a larger downscaling. Again, we have to postpone a final judgement of the reasons for these differences until we have results along a longer trajectory for $UQ^{\bullet-}$. Note that, if we compare our results to the $UQ^{\bullet-}$ data from Ref. [67], the overestimate is a mere 4%. As those data are also 100–250 ppm greater across all components (including Δg_z) than that of Ref. [68], we provisionally assume that the $UQ^{\bullet-}/^i$PrOH data of Ref. [67] overestimates the g-shift components due to an error in calibrating the magnetic field strength in the high-field EPR experiment.

Hyperfine couplings

Hyperfine coupling tensors were calculated for the [4.0 Å + PCM] cluster (distance being defined from the carbonyl oxygens in this case) for 1.99 ps of the trajectory. Isotropic hyperfine coupling constants are presented in Table 4, together with the largest component of dipolar coupling and the Mulliken spin densities, for the oxygen and ring carbon nuclei. Experimental data are taken from various alcoholic solutions, as aqueous data are to the best of our knowledge unavailable. We ignore the inequivalence of the two CO groups and give the hyperfine data for the two $^{13}C_{ipso}$ nuclei as an average over both, rather than for each separately. We do similarly for the $^{17}O_{CO}$ nuclei, the C_{ortho} nuclei with MeO attached, the C_{ortho} with alkyl groups attached, and the nuclei of the methoxy groups. This is because, although the two C_{ipso} centres have measurably different isotropic hyperfine coupling constants [65,69], our simulation's treatment of the asymmetry of the molecule is almost certainly unreliable here. In particular, the strongly asymmetric conformation of the MeO

Table 4 Hyperfine data ([4.0 Å + PCM] cluster results) for ring carbons and oxygens (in MHz)

Position	A_{iso}	$A_{\parallel}$	SD[a]	A_{iso} (exp.)
C_{ipso}	5.1	29.7	167	3.3[b]/2.2[c]
C_{ortho} (C–OMe)	−3.7	10.3	48	–
C_{ortho} (C–Alkyl)	−1.3	12.0	66	(–)1.4[c]
O_{CO}	−17.4	−63.6	201	–
O_{MeO}	2.4	8.4	10	–

[a] Mulliken spin densities (SD) in 10^{-3} a.u.
[b] 2-Propanol solution [65]
[c] Methanol solution [69]

Table 5 Hyperfine data ([4.0 Å + PCM] cluster results) for side-chain C, H (in MHz)

Position	A_{iso}	$A_{\parallel}$	SD[a]	A_{iso} (exp.)
C_{MeO}	1.2	0.8	0.9	<0.3[b]
H_{MeO}	0.6	1.8	0.3	0.1[c]
C_{α}	−3.1	0.7	−5.8	
C_{Me}	−3.0	0.7	−5.3	(–)5.8[b]
C_{Et}	−3.3	0.7	−6.3	
C_{β} (Et)	4.8	1.1	4.2	
H_{α} (Et)	3.5	2.7	1.4	2.8[d]/2.9[c]
H_{α} (Et) (1)	2.1	2.1	0.8	2.1[d]
H_{α} (Et) (2)	4.8	3.2	19.0	3.1[d]
H_{α} (Me)	4.9	2.6	1.9	5.8[d]/6.0[c]

[a] Mulliken spin densities (SD) in 10^{-3} a.u.
[b] Methanol solution [65]
[c] 2-Propanol solution [60]
[d] Ethanol solution [70]

groups is probably an artefact of the short simulation time rather than a reflection of the average conformational situation (we might expect a strong asymmetry of the two MeO groups at any given instant, but not so much when averaged over the whole trajectory).

C_{ipso} HFCs, which are highly sensitive to the solvation environment, are sizeably overestimated, as compared to both isopropanol [69] and methanol [65] solution. However, the $A_{\parallel}$ component is also available experimentally (28.2 MHz for ^{i}PrOH), and this fits our value of 29.7 MHz quite well. Thus, approximately the right amount of spin density is being located at C_{ipso}, but the spin polarization is not described that accurately. We are not aware of any experimental HFCs for C_{ortho} bonded to methoxy groups. HFCs for C_{ortho} bonded to alkyl groups match experimental methanolic data very well.

No experimental data for oxygen coupling constants exist, to our knowledge. We present our data for oxygen HFCs with the note that, in the case of benzosemiquinone, the isotropic ^{17}O coupling constant is significantly underestimated [32], and the same is likely to be true here for the carbonyl oxygen atoms, and possibly for the much smaller HFCs we predict for the methoxy oxygen atoms.

Table 5 presents the data for side-chain HFCs, which are expected to be smaller and far harder to treat accurately, as they arise from a combination of medium-range spin polarization effects and hyperconjugation (discussed below). Our calculations appear to have located too much spin on the methoxy groups, as $A_{\parallel}$ is overestimated for methoxy hydrogen (an experimental value of 0.5 MHz is available for ^{i}PrOH [60]; our value is 1.8 MHz), and the isotropic HFCs are also a little too high. The ^{13}C A_{iso} value for the methyl side-group is significantly too low compared to the experiment. As our A_{iso} value is almost the same for both methyl and the ethyl α-carbon, it is unlikely that the asymmetric configuration is responsible. The A_{iso} values for methyl and ethyl α-protons deviate somewhat from experiment, but our methyl hydrogen $A_{\parallel}$ values seem accurate (2.6 MHz; experimental data is 2.5 MHz in ^{i}PrOH [60]). The ethyl β-carbon data cannot be compared to experiment, as in ubisemiquinone proper this atom is not part of a terminal CH_3 group but part of a long isoprenoid side-chain.

Solvent proton isotropic HFCs are slightly disappointing in that the results are almost identical to those of the benzosemiquinone simulation (Fig. 5)—despite the experimental ^{1}H HFC being 0.8 MHz higher for ubisemiquinone than for benzosemiquinone (1.1 vs. 0.2 MHz in ^{i}PrOH [60]; in water, the $UQ^{\bullet-}$ value is unknown but the $BQ^{\bullet-}$ value is 0.3 MHz [61], essentially the same). In fact, the *highest* solvent proton A_{iso} seen at any point during the $UQ^{\bullet-}$ simulation is 0.7 MHz, lower than the experimental value. This is presumably due to deficiencies in the density functional, leading to an incorrect description of the spin polarization at and spin delocalization onto the solvent proton.

However, the largest anisotropic component of the solvent protons, $A_{\parallel}$, is reproduced better. If we plot a frequency

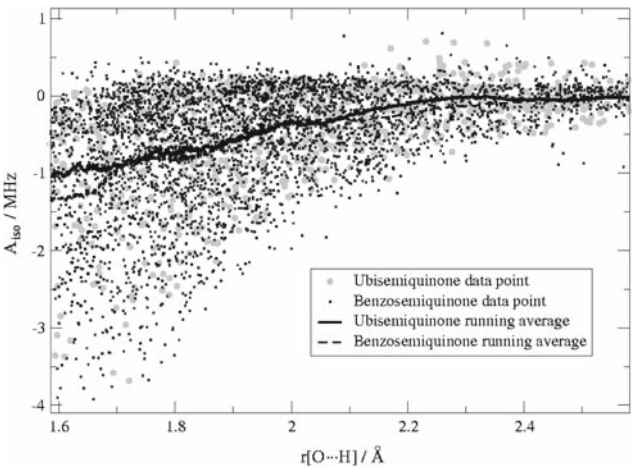

Fig. 5 Solvent proton isotropic HFCs for both ubi- and benzosemiquinone

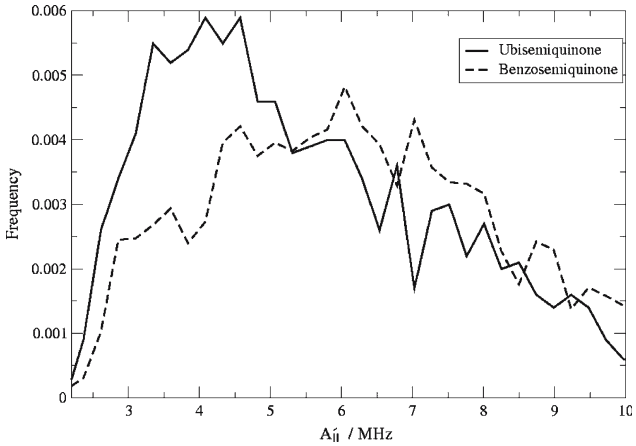

Fig. 6 Frequency chart for solvent proton $A_{\parallel}$ values for ubi- and benzosemiquinone

graph of $A_{\parallel}$ (Fig. 6), we see that it peaks at about 6 MHz for our benzosemiquinone simulation (experimental: 5.9 MHz in ^{i}PrOH [60], 6.0 MHz in H_2O [61]) and 4.6 MHz for ubisemiquinone (experimental: 4.7 MHz in ^{i}PrOH [60]). This parameter is dominated by dipolar coupling with the p-shaped lobes of the spin density around the carbonyl oxygen atoms, and thus the accuracy with which we calculate it seems to indicate that our calculations have reproduced r[O···H] and the amount of spin density at oxygen reasonably well.

Spin hyperconjugation

The spin densities on the β-carbons of the side chains (the CH_3 carbons in Et and OMe) cannot be explained merely in terms of spin polarization, but indicate a certain amount of hyperconjugation of the SOMO with β-carbon σ-orbitals. Table 6 shows the Mulliken spin densities of the side chain heavy nuclei and the *ortho*-carbons. We can see that the positive spin density on the π-system induces a small negative spin density on the methyl carbon and the α-carbon of the ethyl group. Spin polarization of the C–C bond would then be expected to induce an even smaller, positive spin density at the ethyl β-carbon. In fact, while the spin density at the β-carbon is positive, it is surprisingly large, almost the magnitude of the spin density at the α-carbon. The effect on the

Table 6 Time-average atomic spin densities for *ortho*-carbons and the α and β atoms of their substituents ([4.0 Å + PCM] cluster results)

Substituent	C_{ortho}	C/O_{α}	C_{β}
OMe(1)	32.9	5.8	0.9
OMe(2)	63.6	14.5	0.8
Me	59.3	−5.3	–
Et	73.2	−6.3	4.2

Mulliken spin densities, given in 10^{-3} a.u.

Table 7 Variation of side-chain β-carbon hyperfine couplings with dihedral angle ([4.0 Å + PCM] cluster results)

τ/°[a]	A_{iso} / MHz		
	MeO(1)	MeO(2)	Et
0–15°	−1.8	−1.8	–
15–45°	0.2	0.1	1.6
45–75°	0.7	2.2	4.2
75–90°	1.8	1.9	4.4

[a] As we are concerned here only with whether the side group is perpendicular or in-plane, angles of $\tau > 90°$ have been treated as $(180 - \tau)$ and $\tau < 0$ as $|\tau|$

HFC is even more pronounced, with (according to our calculations) A_{iso} being *larger* for the β- than for the α-carbon. An even stronger indication of hyperconjugation is the positive spin densities on the methoxy carbons. A small positive spin density arises at the methoxy oxygens, which is unsurprising, as resonance structures can be constructed with an unpaired electron at these centres. Spin polarization should then locate negative spin density on the methoxy carbon nuclei. In fact, however, the spin density at the carbons is *positive*—albeit rather small, as spin polarization partially cancels the effect of hyperconjugation. (In the case of ethyl β-carbon, both spin polarization and hyperconjugation act in concert to increase spin density.)

As hyperconjugation involves an interaction with a π-system made up of p-orbitals perpendicular to the ring, the degree of hyperconjugation—and hence the HFCs—strongly depends on the conformation of the substituent. This may be seen from Table 7, which shows how the β-carbon HFCs vary with dihedral angle. When the substituents are in-plane, the HFCs are as would be expected from spin-polarization effects alone: the Et β-carbon HFC is far smaller, and the methoxy carbon HFCs become negative at low dihedral angles. These HFCs, then, evidently need an accurate treatment of conformational motion to properly compute. It should also be noted that the B3LYP method we use is possibly *over*estimating the strength of hyperconjugation, as the methoxy carbon and hydrogen A_{iso} values, as well as the ^{1}H $A_{\parallel}$ values, are too high compared with the experiment (see earlier), indicating that too much spin density has been located in the area. (It is also possible that the problem lies in the conformation—that the conformation adopted in our simulation has the MeO groups more perpendicular than they should be on average, due to short simulation time.)

4 Conclusion

Application of ab initio molecular dynamics techniques to aqueous ubisemiquinone radical anion has allowed us to

assess the effects of dynamics on the EPR parameters, the degree to which solvation spheres beyond the first play a role in the *g*-tensor, and the effects, in a dynamical environment, of the H-bonds to methoxy oxygen atoms. Additionally, while our simulation is as yet too short to make authoritative statements about the preferred conformation of the side-chains in solution, it does indicate that conformations with one methoxy group pointed "inwards" and one "outwards" are at least stable, as our simulation showed no inclination of leaving this state. This is in contrast to static calculations which tend to predict a conformation of both methoxy groups "outwards". As in our prior investigations on benzosemiquinone [18,19], the agreement with experimental *g*-tensors is not improved by inclusion of dynamics, with static calculations evidently benefitting from error compensation. Our investigation has also identified the importance of hyperconjugation in the spin density distribution on the side groups, indicating the importance of conformation in any theoretical consideration of side-chain HFCs.

The present simulations have provided an unprecedentedly detailed dynamical view of the ubisemiquinone radical anion and of its EPR parameters in aqueous solution. The simulation will be extended, so as to more fully sample the conformational phase space of this important bioradical. Such simulations in aqueous solution will subsequently be used to validate classical force fields or QM/MM methodology that may be applied also to ubisemiquinone radical anions in biological surroundings.

Acknowledgments The MD simulations have been performed on the federal high-performance supercomputing facilities at the Leibniz Rechenzentrum in München. We thank Dr. Nikos Doltsinis for support and technical assistance with the MD aspects of our research.

References

1. Patai S (1974) Chemistry of quinoid compounds. Interscience, New York
2. Trumpower B (ed) (1982) Functions of quinone in energy conserving systems. Academic Press, New York
3. Morton R (ed) (1965) Biochemistry of quinones. Academic Press, New York
4. Levanon H, Möbius K (1997) Annu Rev Biophys Biomol Struct 26:495
5. Prisner T, Rohrer M, MacMillan F (2001) Annu Rev Phys Chem 52:279
6. Kaupp M, Bühl M, Malkin VG (2004) Calculation of NMR and EPR parameters. Wiley-VCH, Weinheim
7. Munzarová ML (2004) DFT calculation of EPR hyperfine coupling tensors. In: Calculation of NMR and EPR parameters. Wiley-VCH, Weinheim
8. O'Malley PJ (1997) J Phys Chem A 101:6334
9. O'Malley PJ (1998) J Phys Chem A 102:248
10. O'Malley PJ (1998) J Am Chem Soc 120:5093
11. Eriksson LA, Himo F, Siegbahn PEM, Babcock GT (1997) J Phys Chem A 101:9496
12. Himo F, Babcock GT, Eriksson LA (1999) J Phys Chem A 103:3745
13. Grafton AK, Wheeler RA (1997) J Phys Chem A 101:7154
14. Boesch SE, Wheeler RA (1997) J Phys Chem A 101:5799
15. Wise KE, Grafton AK, Wheeler RA (1997) J Phys Chem A 101:1160
16. Nonella M (1998) Photosynth Res 55:253
17. Zhan C-G, Chipman DM (1998) J Phys Chem A 102:1230
18. Nonella M (1998) J Phys Chem B 102:4217
19. Fiedler S, Eloranta J (2005) Mag Res Chem 43:231
20. Kaupp M (2003) Ab initio and density functional calculations of electronic *g*-tensors for organic radicals. In: Lund A, Shiotani MEPR spectroscopy of free radicals in solids: trends in methods and applications (progress in theoretical chemistry and physics). Kluwer, Dordrecht
21. Kaupp M, Remenyi C, Vaara J, Malkina OL, Malkin VG (2002) J Am Chem Soc 124:2709
22. Kaupp M (2002) Biochemistry 41:2895
23. Kacprzak S, Kaupp M (2004) J Phys Chem B 108:2464
24. Sinnecker S, Reijerse E, Neese F, Lubitz W (2004) J Am Chem Soc 126:3280
25. Ciofini I, Reviakine R, Arbuznikov A, Kaupp M (2004) Theor Chem Acc 111:132
26. Kacprzak M, Kaupp M, MacMillan F (2006) J Am Chem Soc 128:5659
27. Epel B, Niklas J, Sinnecker S, Zimmermann H, Lubitz W (2006) J Phys Chem B 110:11549
28. Fritscher J, Prisner TF, MacMillan F (2006) Appl Magn Reson 30:251
29. Car R, Parrinello M (1985) Phys Rev Lett 55:2471
30. Asher JR, Doltsinis NL, Kaupp M (2004) J Am Chem Soc 126:9854
31. Asher JR, Doltsinis NL, Kaupp M (2005) Mag Res Chem 43:S237
32. Asher JR, Kaupp M (2007) ChemPhysChem 1:69
33. Pavone M, Cimino P, De Angelis F, Barone V (2006) J Am Chem Soc 128:4338
34. Pavone M, Benzi C, De Angelis F, Barone V (2004) Chem Phys Lett 395:120
35. Pavone M, Cimino C, Crescenzi O, Sillanpaeae A, Barone V (2007) J Phys Chem B 111:8928
36. Takase H, Kikuchi O (1994) Chem Phys 181:57
37. Igarashi M, Ishibashi T, Tachikawa H (2002) THEOCHEM 594:61
38. Tachikawa H, Igarashi M, Ishibashi T (2002) Chem Phys Lett 352:113
39. Ramirez R, Schulte J, Boehm MC (2005) Chem Phys Lett 402:346
40. Schulte J, Boehm MC, Lopez-Ciudad T, Ramirez R (2004) Chem Phys Lett 389:367
41. Yazyev OV, Helm L (2006) Theor Chem Acc 115:190
42. CPMD code, v. 3.7.1. Copyright IBM Corp 1990–2006, Copyright MPI für Festkörperforschung, Stuttgart 1997–2001. Availability and further information at www.cpmd.org
43. Becke A (1998) Phys Rev A 38:3098
44. Lee C, Yang W, Parr R (1988) Phys Rev B 37:785
45. Sprik M, Hutter J, Parrinello M (1996) J Chem Phys 105:1142
46. Kuo I-FW, Mundy CJ, McGrath M, Siepmann JI, VandeVondele J, Sprik M, Hutter J, Chen B, Klein ML, Mohamed F, Krack M, Parrinello M (2004) J Phys Chem B 204:12990
47. Troullier N, Martins JL (1993) Phys Rev B 43:1993
48. Ahlrichs R, Bär M, Häser M, Horn H, Kölmel C (1999) Chem Phys Lett 162:165
49. Ahlrichs R, von Arnim M (1995) In: Clementi E, Corongiu G (eds) Methods and techniques in computational chemistry: METECC-95. Club Européen MOTECC
50. Perdew J, Wang Y (1986) Phys Rev B 33:8822
51. Godbout N, Salahub D, Andzelm J, Wimmer E (1992) Can J Chem 70:560
52. Becke A (1993) J Chem Phys 98:5648

53. Stephens PJ, Devlin FJ, Chabalowski CF, Frisch MJ (1994) J Phys Chem 98:11623
54. Barone V (1995) In: Chong D (ed) Recent advances in density functional methods. World Scientific, Singapore
55. Malkin VG, Malkina OL, Reviakine R, Arbuznikov AV, Kaupp M, Schimmelpfennig B, Malkin I, Repiský M, Komorovský S, Hrobarik P, Malkin E, Helgaker T, Ruud K, MAG-ReSpect, v. 2.1, 2005
56. Malkina OL, Vaara J, Schimmelpfennig B, Munzarová ML, Malkin VG, Kaupp M (2000) J Am Chem Soc 122:9206
57. Kaupp M, Reviakine R, Malkina OL, Arbuznikov A, Schimmelpfennig B, Malkin VG (2002) J Comput Chem 23:794
58. Hess BA, Marian CM, Wahlgren U, Gropen O (1996) Chem Phys Lett 251:365
59. Sinnecker S, Reijerse E, Neese F, Lubitz W (2004) J Am Chem Soc 126:3280
60. MacMillan F, Lendzian F, Lubitz W (1995) Mag Res Chem 33:S81
61. Flores M, Isaacson R, Calvi R, Feher G, Lubitz W (2004) J Am Chem Soc 126:3280
62. O'Malley P (1998) Chem Phys Lett 285:99
63. Nilsson JA, Lyubartsev A, Eriksson LA, Laaksonen A (2001) Mol Phys 99:1795
64. Nonella M (1998) J Phys Chem B 102:4217
65. Samoilova RI, Gritsan NP, Hoff AJ, van Liemt WBS, Lugtenburg J, Spoyalov AP, Tsvetkov YD (1995) J Chem Soc Perkin Trans 2:2063
66. Klamt A, Schüürmann G (1993) J Chem Soc Perkin Trans 2:799
67. Burghaus O, Plato M, Rohrer M, Möbius K (1993) J Phys Chem 97:7639
68. Nimz O, Lendzian F, Boullais C, Lubitz W (1998) Appl Magn Res 14:255
69. Isaacson R, et al (1996) In: Michel-Beyerle M-E (ed) The reaction centre of photosynthetic bacteria, structure and dynamics. Springer, Berlin
70. Lehtovuori P, Joela H (2000) J Mag Res 145:319